 MCB, vol.5, no.1, pp.9-18, 2008

Blood Flow Patterns in the Proximal Human Coronary Arteries: Relationship to Atherosclerotic Plaque Occurrence

Jin Suo*, John N. Oshinski*,† and D.P. Giddens*‡

Abstract: Atherosclerotic plaques in human coronary arteries are focal manifestations of systemic disease, and biomechanical factors have been hypothesized to contribute to plaque genesis and localization. We developed a computational fluid dynamics (CFD) model of the ascending aorta and proximal sections of the right and left coronary arteries of a normal human subject using computed tomography (CT) and magnetic resonance imaging (MRI) and determined the pulsatile flow field. Results demonstrate that flow patterns in the ascending aorta contribute to a pro-atherosclerotic flow environment, specifically through localization of low and oscillatory wall shear stress in the neighborhood of coronary orifices. Furthermore, these patterns differ in their spatial distribution between right and left coronary arteries. Entrance effects of aortic flow diminish within two vessel diameters. We examined relationships between spatial distributions of wall shear stress and reports of plaque occurrence in the literature. Results indicate low wall shear stress is co-located with increased incidence of lesions, and higher wall shear stresses are associated with lesion-resistant areas. This investigation does not consider plaque progression or advanced lesions, inasmuch as the CFD model was developed from a normal individual and the clinical data used for comparisons were obtained from autopsy specimens of subjects who died from non-cardiovascular causes. The data reported are consistent with the hypothesis that low wall shear stress is associated with the localization of atherosclerotic lesions, and the results demonstrate the importance of aortic flow on flow patterns in the proximal segments of the coronary arteries.

* Wallace H. Coulter Department of Biomedical Engineering at Georgia Tech and Emory, Atlanta, GA 30332

† Department of Radiology, Emory University School of Medicine, Atlanta, GA 30322

‡ Corresponding author. Third Floor, Tech Tower, Georgia Institute of Technology, Atlanta, GA 30332-0363. Email: don.giddens@coe.gatech.edu

1 Introduction

Cardiovascular disease is the leading killer among all racial and ethnic groups in the United States (1) with atherosclerosis being the most common manifestation. Ischemic heart disease results from obstruction of blood flow to the heart, usually caused by atherosclerotic plaques in the coronary arteries. It has long been observed that orifice regions and entrance sections of both the right and left coronary arteries are favorite sites for atherosclerotic plaques (2). Investigation of atherosclerotic lesion distribution in aortas at autopsy from 109 male subjects who died from non-cardiovascular causes demonstrated a relatively high occurrence of lesions at the proximal inflow tracts of major branch vessels (3). Plaque distributions based on autopsy of 50 individuals who died of non-cardiovascular causes were found to be asymmetrical about the circumference of the coronary arteries, with atheroma being more concentrated on the myocardial side in the proximal segment of the right coronary artery, but more toward the epicardial side in the left coronary artery (4). In another study of 270 subjects who died of accidental causes, a region between the orifice and the main bifurcation of the left coronary arteries was identified which had a "natural resistance" to atherosclerosis by comparison to atherosclerotic involvement in the distal and proximal segments of the left main coronary artery (5). Observations such as these have led to the hypothesis that flow patterns in proximal segments of major coronary arteries have a causative influence on the specific

localization of atherosclerotic disease.

However, *in vivo* investigation of blood flow in coronary arteries and its interaction with the vessel wall has been a challenge. The coronary arteries are deep inside the body, are relatively small in size, and blood flow in the main trunks may be influenced by the complex flow in the aortic root (6), the source of coronary artery blood supply. Noninvasive methods of study are limited, both with regard to hemodynamic variables and biological markers of plaque development. This report is part of an ongoing investigation of hemodynamics and atherosclerosis in human coronary arteries that focuses on integrating several methodologies in an effort to understand the causes of plaque initiation, progression and rupture. Attention is placed upon the proximal regions of the major coronary arteries, and due to the large interest in fluid dynamic wall shear stress (WSS) as an important factor, emphasis in this study is upon this hemodynamic variable. The WSS is derived from modeling flow in the coronary arteries of individual subjects using a combined methodology that includes computational fluid dynamics (CFD), computed tomography (CT) and magnetic resonance imaging (MRI). In the modeling approach, MRI slices from human subjects provide geometric data for the aorta. Because of spatial resolution capabilities, the coronary arteries are scanned separately using a CT scanner so as to improve geometric modeling, and the velocity boundary condition data are derived from phase contrast PC-MRI, all of which are combined to provide a joint model of the aorta and the coronary arteries for the CFD calculation. Since the purpose of this investigation is to study the proximal coronary arteries and because previous studies (6) have shown an influence of aortic flow upon the entrance regions of these vessels, it was deemed necessary to incorporate the aorta into the CFD model.

2 Methods

Imaging. Computed tomography (CT) imaging of a volunteer was performed on a 16-slice spiral CT scanner (General Electric Medical Systems,Waukesha, WI). ECG-gating and retrospective, multi-sector reconstruction was employed. The CT scan covered an area from the apex/inferior wall of the heart to the top of the aortic arch during a 15second breath-hold. CT imaging was done during a contrast injection of 80 cc of contrast agent at 4cc/sec. Image resolution was 0.6 by 0.6 mm in plane, and slice thickness 0.625 mm (Figure 1). This spatial resolution ensures accurate reconstruction of the major lumens of the coronary arteries, where the diameter is typically 3-4 mm. Although CT scanning has high resolution in describing the geometric structures of the vessels, the technique cannot provide flow information. However, by using PC-MRI scanning at appropriate sections of the aorta and coronary arteries one can obtain reliable information on flow rates through these vessels, data necessary for CFD calculations.

MRI scanning has lower resolution than CT, but this non-invasive technique can be used to accurately image large arteries of most subjects. Because the thoracic aorta is approximately 25 mm in diameter, MRI can provide geometric information of the aorta with the same relative resolution as the CT slices of coronary arteries. A stack of 44 transverse images was acquired in a separate volunteer using a 1.5T scanner (Philips Medical Systems, Best, Netherlands). Images were acquired using a navigator echo-gated whole heart protocol (7). Each image has 256×256 pixels in a view of 350×350 mm with a thickness of 3 mm. The slices were contiguous and covered the ascending aorta, the aortic arch and the proximal descending aorta. The slices provided geometric information of the aorta for construction of the CFD model.

After acquiring the scans for determining aortic geometry, PC-MRI was performed at three locations in the aorta to obtain time-resolved velocity distributions. Twenty velocity images equally-spaced over the cardiac cycle were acquired. The first section, or model inlet section, was located at the aorta root where three orthogonal velocity components were measured. The second section crossed the descending aorta where the outlet section of the model was located, and the axial velocity was obtained at this section. The third section was approximately midway in the ascend-

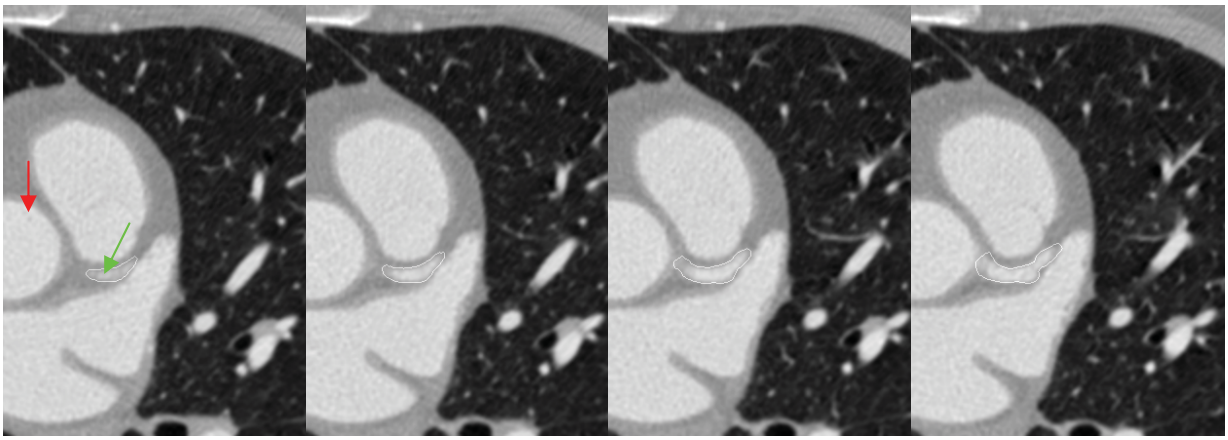

Figure 1: Example CT slices of the aortic root (red arrow) and the left coronary artery (green arrow). Serial slices such as these are employed in constructing the CFD model geometry.

ing aorta, and it was employed as a "test section" for validation of the computational results, i.e., if the CFD simulation is accurate, computations would produce the same velocity distribution as the PC-MRI result at that section (6). Navigator echo-gated, PC-MRI was also performed in the RCA, LAD and LCX, providing time-resolved flow waveforms for the coronary arteries. In the coronary arteries, 10 time frames were acquired over the cardiac cycle. Details on the scan protocol are described in detail elsewhere (8). The study was approved by the IRB of Emory University and all patients provided written informed consent.

CFD model. Image segmentation is necessary to find the edge of an arterial lumen on the CT and MRI images, and the methodology employed is described elsewhere (6). Serial contours in space that form the boundaries of the lumens of the aorta and coronary arteries were produced by the segmenting process. The model of the aorta and the models of the coronary arteries with smoothed surfaces were reconstructed from the serial spatial contours.

The final CFD model was composed of a model combining the aorta and the coronary arteries. The procedure for assembling these separate models was based on the relative orientation of the main trunks of the coronary arteries to the aortic root as obtained from the MRI scans. Although the MRI images cannot provide high resolution geometric descriptions of the boundary of the coronary lumens, the centers of the main trunks of the coronary arteries can be estimated in MRI slices. These centers determined the relative orientations of the proximal segments of the coronary arteries to the aortic root, and then the models of coronary arteries that were constructed from CT slices were aligned according to these orientations and combined with the aorta model. The complete CFD model is shown in the upper panel of Figure 2.

Governing Equations. The incompressible continuity and Navier-Stokes equations were employed as the governing equations, and these were solved numerically using the commercial software package, CFD-ACE, as described in (6).

Boundary conditions. It is impractical to obtain PC-MRI velocity data for three velocity components at all boundaries of the computational model due to the length of time required for a subject to be in the scanner. The inlet section of the ascending aorta is more important for the boundary conditions because this section is across the aortic root and very close to the ostia of coronary arteries, where the complex aortic flow is expected to influence the entry flow patterns of the coronary arteries. At this section, the pulsatile 3D velocity distribution of blood flow obtained from PC-MRI scanning *in vivo* was transferred as the boundary condition directly, with 20 such 3D velocity distributions over one cardiac cycle estab-

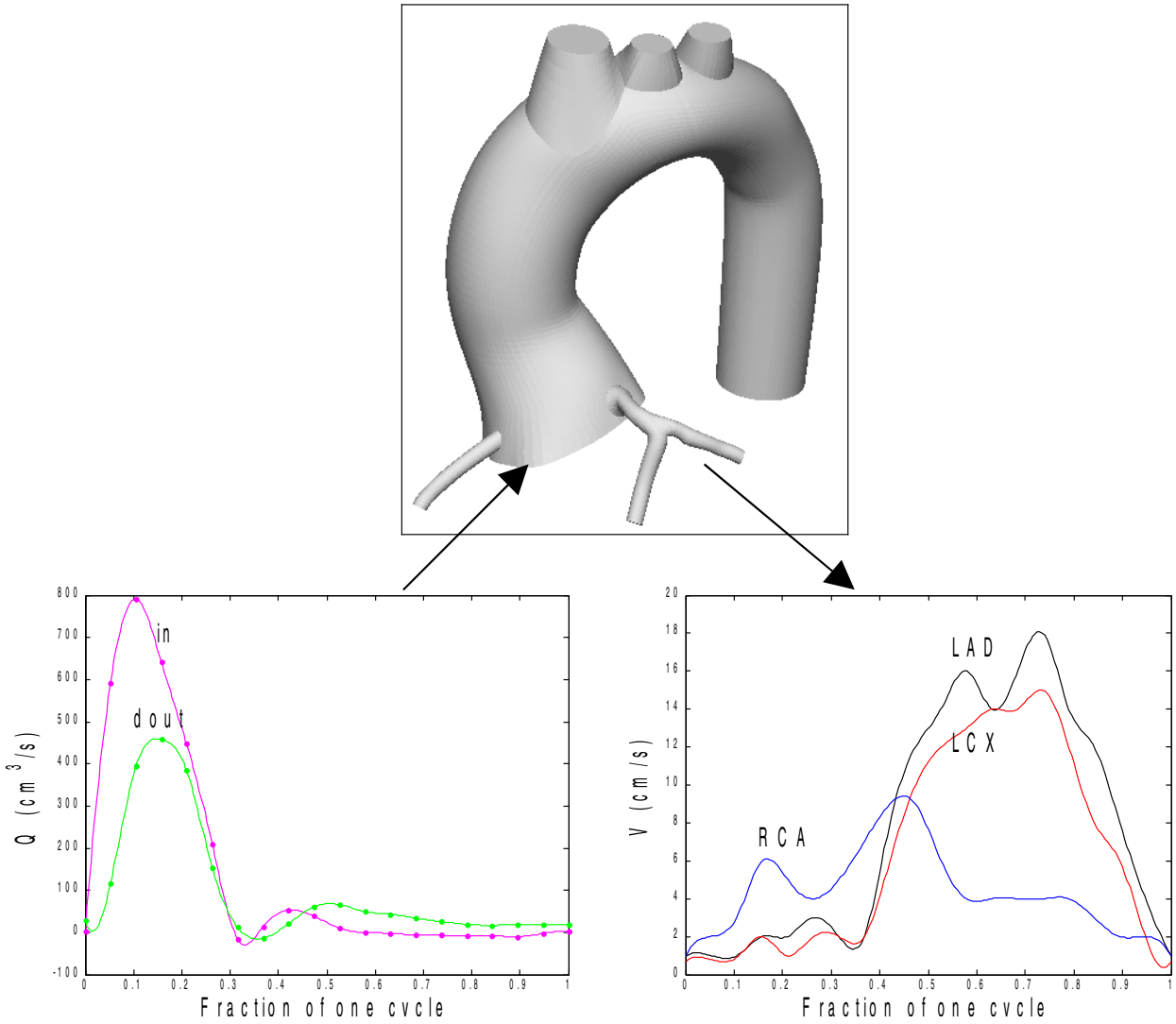

Figure 2: The CFD model and the boundary conditions. The top panel shows the geometry of the complete model employed for the computational grid. The bottom left panel presents the flow waveforms at the inlet (near aortic root) and outlet sections (descending thoracic aorta), while the lower right panel provides the flow waveforms for the left circumflex (LCX), left anterior descending (LAD) coronary arteries and the flow waveform for the right circumflex artery (RCA). Flow wave forms are obtained from PC-MRI measurements.

lishing the boundary conditions in this inlet section. At the boundary marking the descending aortic outflow, only the axial velocity component from the PC-MRI measurements was employed. The flow waveforms obtained by integrating the axial velocity distributions over the two boundary sections are shown in the lower left of Figure 2 where the time for one cardiac cycle is normalized to be 1. The difference in flow waveforms between inlet and outlet sections of the aorta was distributed into the branches emanating from the aortic arch assuming traction-free conditions at their outlets, thus imposing the assumptions that the outflow velocity in each arch vessel is along the normal direction and the axial velocity gradients are zero.

The flows emanating from the coronary arteries were imposed using the velocity waveforms obtained from PC-MRI scanning. The slice thickness (6 mm) of the PC-MRI scans of the coronary

arteries was larger than the diameter of the lumen (∼3-4 mm) so that the slices provided a good estimate of mean velocities across the sections at different times, but not velocity distributions or profiles within the section. The velocity waveforms for the RCA, LAD and LCX are shown in the lower right panel of Figure 2.

3 Results

Entrance Flow Patterns in the Proximal RCA and LM. Computed entrance flows in the right and left coronary arteries behave differently. Figure 3 shows the entrance axial velocity profiles at times representing 0.2 to 0.6 fractions of one cardiac cycle, in increments of 0.1. Referring to Figure 2, this period covers the late stages of systole, where flow into the coronary arteries is low, through early to mid diastole, where flow increases to its maximum in the coronary vessels. In the RCA, there is near wall flow reversal during late systole on the myocardial side of the lumen, and flow is skewed toward the epicardial side. In contrast, the LM experiences skewing of the velocity profile toward the myocardial wall during this period, with a near wall reversal occurring at the epicardial wall. Thus, while the neighborhoods of the two vessel orifices contain areas of oscillating WSS that when time-averaged over the cardiac cycle are relatively low, these areas are localized differently: the RCA has this characteristic along the myocardial wall, and the LM experiences the phenomenon along its epicardial side. These differences arise primarily from the complex flow patterns in the ascending aorta (6) from which the coronary vessels derive their flow.

Interestingly, this strongly asymmetric behavior did not persist very far beyond the entrances of the LM and RCA. After about 5mm, the near wall flow reversal was not present and flow was generally unidirectional until it encountered a branch (LAD/LCX), thus suggesting that a longer LM section in a given individual would tend to have relatively less area exposed to WSS patterns that have been associated with atherogenesis than would a shorter LM vessel.

Patterns of WSS in the LCA. The patterns computed for WSS magnitude from the CFD results are shown at several representative times for the LCA in Figure 4(a): peak aortic flow (t = 0.1, see the flow waveforms in Figure 2); late systole (t = 0.25); aortic valve closure time (t = 0.4); early diastole (t = 0.55); peak coronary flow time (t = 0.7); and late diastole (t = 0.85). At t = 0.1, the entry section of the LCA is influenced by strong aortic flow patterns (see (6)), and WSS can exceed 50 dynes/cm^2 in the epicardial side of the ostium, even though there is almost no net flow into the LAD and LCX at this time. Following peak aortic flow, the high WSS in the entry section becomes much reduced, and the WSS in the LAD and LCX continues to be very low later in systole (t = 0.25). When the aortic valve closes at t = 0.4, the flow into the LCA begins to accelerate and the WSS increases in the LAD and LCX, although the highest WSS is only about 15 dynes/cm^2 during this period. In the first half of diastole (t = 0.55 and 0.7), flows into the LAD and LCX increase to their peak values, bringing WSS to approximately 50 dynes/cm^2 on the myocardial side of the middle section of the LM. Although the WSS is about 20 dynes/cm^2 in much of the LM, LAD and LCX during this time, some regions continue to experience WSS less than 10 dynes/cm^2: the myocardial side of the LM just upstream of the bifurcation, both outer sides of the bifurcation, and two regions in the LCX. WSS then decreases in late diastole (t = 0.85) because the flow decreases.

Figure 4(b) presents the mean WSS distribution for the LCA, defined as the time average at each spatial location. Two regions with higher WSS than their neighborhoods can be seen. The first, the main region of high WSS in the left coronary artery, is located in the first half of LM and skewed toward the myocardial side. Another region is concentrated in a small area near the flow divider of the bifurcation.

4 Discussion

Atherosclerosis can be characterized as a systemic disease with focal manifestations, and this latter phenomenon has been a motivation for numerous studies of the role of biomechanics in the genesis and pathophysiology of this disease.

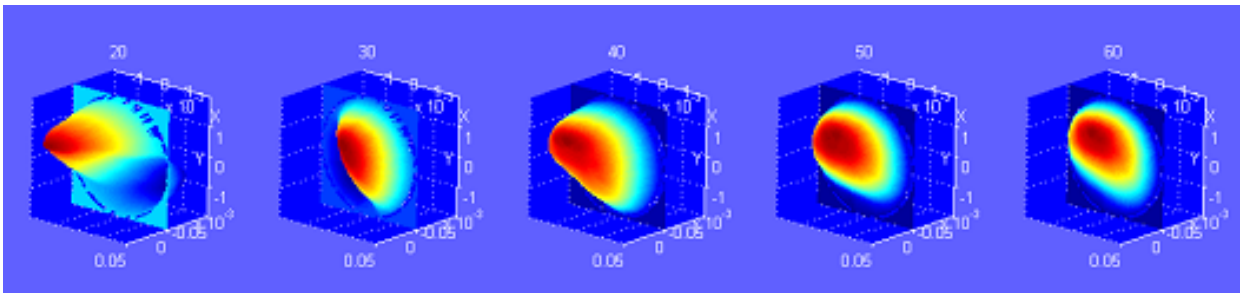

Figure 3A: Axial velocity profiles at a station near the entrance of the right coronary artery (RCA) at time t = 0.2, 0.3, 0.4, 0.5, 0.6 (See Figure 2). Reverse velocities can be seen along the myocardial wall during systole, created by a strong vortex pattern in the ascending aorta.

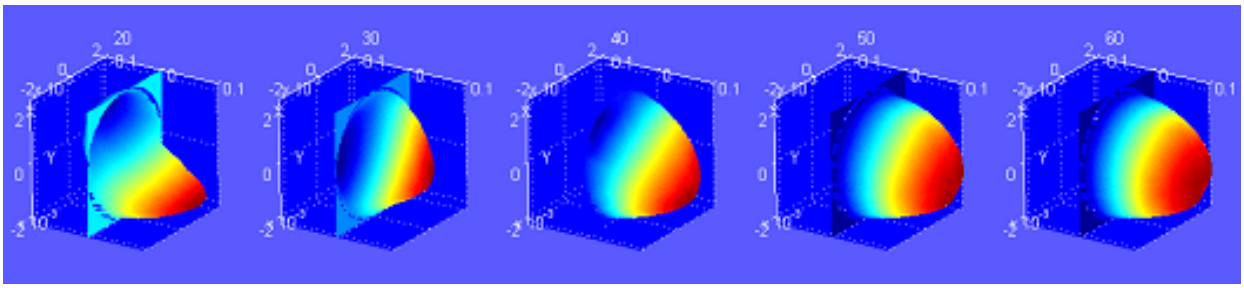

Figure 3B: Axial velocity profiles at a station near the entrance of the left main coronary artery (LM) at corresponding times during the cycle. In contrast to the RCA, reverse velocities occur along the epicardial side of the vessel.

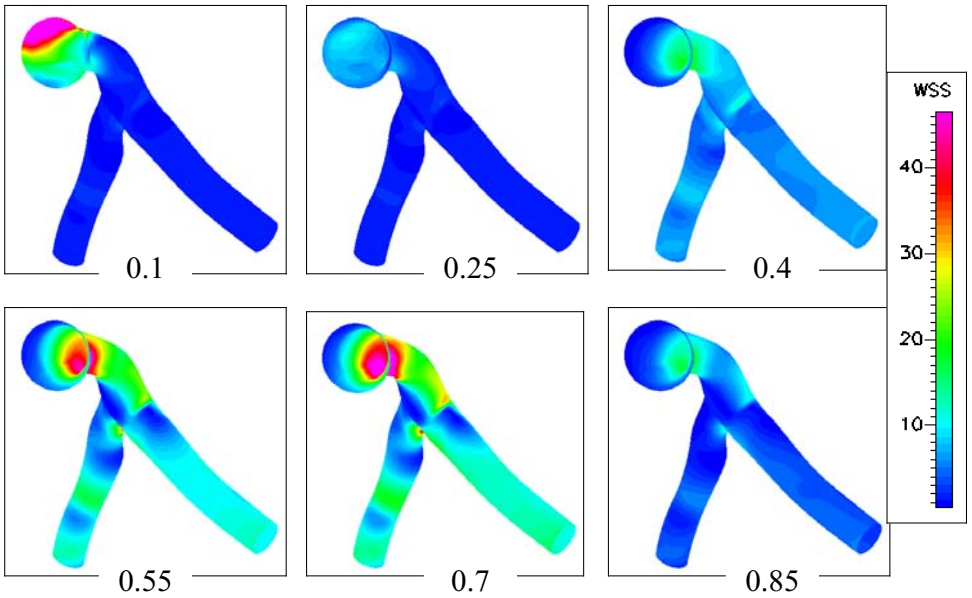

Figure 4(a): Patterns of WSS magnitude at several different times over one cardiac cycle. The number under each panel is based on a normalized time (see Figure 2), and the units of the color bars are dynes/cm^2.

$$WSS_{i,j} = (WSS^{1}_{i,j} + WSS^{2}_{i,j} + \cdots + WSS^{20}_{i,j})/20$$

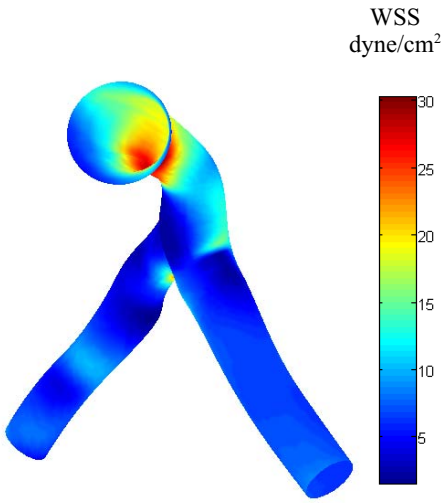

Figure 4(b): Distribution of WSS magnitude computed from WSS distributions of every surface point (i,j) at 20 points of time in the cycle. The units of the color bars are dynes/cm^2.

The high incidence and critical consequences of coronary artery disease make investigations of the coupling of biomechanics and pathophysiology in these vessels particularly relevant. Autopsy studies have demonstrated that the majority of thin-cap fibroatheromas (TCFAs), plaque ruptures, and healed plaque ruptures are located in the proximal coronary arteries (9-11). Futhermore, angiographic studies of patients with ST-segment elevation myocardial infarction have demonstrated that angiographically identified plaque ruptures are clustered within the proximal third of each of the epicardial coronary vessels (12,13).

Considerable evidence accumulated by numerous investigators indicates that relatively low mean WSS, which usually occurrs in concert with strong directional changes in WSS vectors, induces pro-atherogenic reactions by endothelial cells and in animal models. Low WSS is known to lead to increases in monocyte adhesion and binding to endothelial cells, increases in endothelial cell layer permeability to macromolecules, augmented endothelial cell apoptosis, and stimulation of endothelial cell production of reactive oxygen species (14). Vascular adhesion molecule 1 is increased in areas of low WSS in the mouse aorta (15) and increased expression of pro-atherogenic inflammatory mediators with development of atherosclerotic plaque rich in lipid core and relatively devoid of collagen and smooth muscle cells has been observed in areas of low WSS in the carotid arteries of apoE -/- mice (16). Early clinical evidence of the association of low (i.e., <10 dynes/cm^2) WSS and atherosclerosis is reported in the human aorta and the common carotid circulation using magnetic resonance imaging (17,18). High WSS (i.e., >70 dynes/cm^2), on the other hand, can also produce endothelial damage (19), promote platelet deposition (20), and possibly plaque rupture (21,22). In the intermediate range (i.e., approximately 10-70 dynes/ cm^2), WSS is thought to be atheroprotective (23).

To date, there is little known from *in vivo* human studies in the coronary circulation that evaluate the role of WSS in the spectrum that includes plaque initiation, progression and transformation to the most common vulnerable phenotype, TCFAs. Our research methods are aimed at providing accurate descriptions of the hemodynamic flow field, including estimates of WSS, in individual subjects using noninvasive or minimally invasive methods. Obtaining the corresponding biological and clinical results *in vivo* remains challenging, but advances in tissue and molecular imaging may soon provide such data. Ultimately, the objectives are to elucidate biomechanics-related mechanisms of atherosclе-

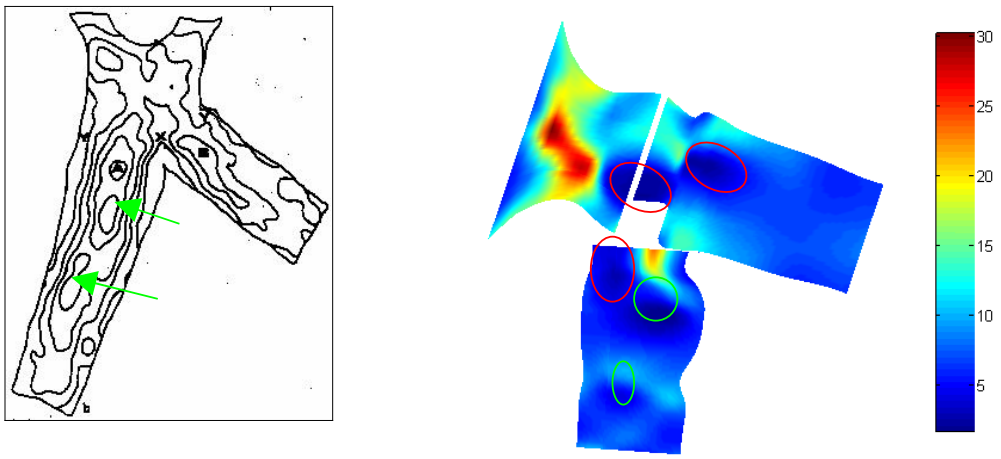

Figure 5: From the open state, the regions of low WSS appear to be linked to the regions of high frequency of plaques observed by Svindland (24). This correspondence is consistent with the hypothesis that low and oscillating WSS is a localizing factor for atherosclerosis in the coronary arteries.

rotic plaque pathophysiology and to translate this knowledge to clinical usefulness.

Comparison of Computed WSS with Observations of Plaque Localization. Svindland (24) studied the localization of early sudanophilic and fibrous plaques in the main stem and proximal branches of opened and stained left coronary arteries from autopsies of subjects who died from trauma. The distribution of sudanophilic and fibrous plaques in 41 arteries was represented by contour lines connecting points with equal frequency of lesions (see left panel of Figure 5). Three regions with higher frequency of lesions were marked (see ▲ ■, and × in Figure 5), which are both outer sides of the bifurcation and the myocardial side upstream of the bifurcation. As these results were presented in an open lumen state, we opened our mean WSS model (Figure 4(b)) in a similar fashion to make a comparison, shown in the right panel of Figure 5. From the open state display, the regions with low WSS marked by red contours in the mean WSS model appear to be linked to the regions of high frequency of plaques in Svindland's results; and the two areas marked by green contours in the WSS model appear to correspond to the two distal areas of higher incidence in the Svindland observations, marked by green arrows.

Velican, C. and Velican, D. (5) examined 270 subjects who died of accidental causes and investigated the distribution of atherosclerosis in the coronary arteries in these subjects. They observed that in subjects of similar age, sex and branching anatomical pattern, and in the presence of similar risk factors for coronary heart disease, the first centimeter distal to the aortic origin of both left and right coronary arteries behaves differently than the second and third centimeters (the right panel in Figure 6). These investigators concluded that the middle segment of the left main coronary artery that is beyond about one centimeter distal to the ostium is more resistant to intimal thickening and plaque development than the orifice region and the main bifurcation region. These observations and conclusions are consistent with our hemodynamic calculations and the hypothesis of higher WSS being atheroprotective.

Implications of the Study. Comparisons of WSS obtained from a single individual and plaque localization data from autopsies have obvious limitations. Nonetheless, several findings in this study support the hypothesis that low mean WSS, typically accompanied by oscillatory WSS vectors, provides an *in vivo* environment in the coronary arteries that promotes atherosclerotic plaque localization. The study also can be used to "predict" where early coronary artery plaques will occur, and these predictions can be subjected to scrutiny through examination of autopsy and imaging studies.

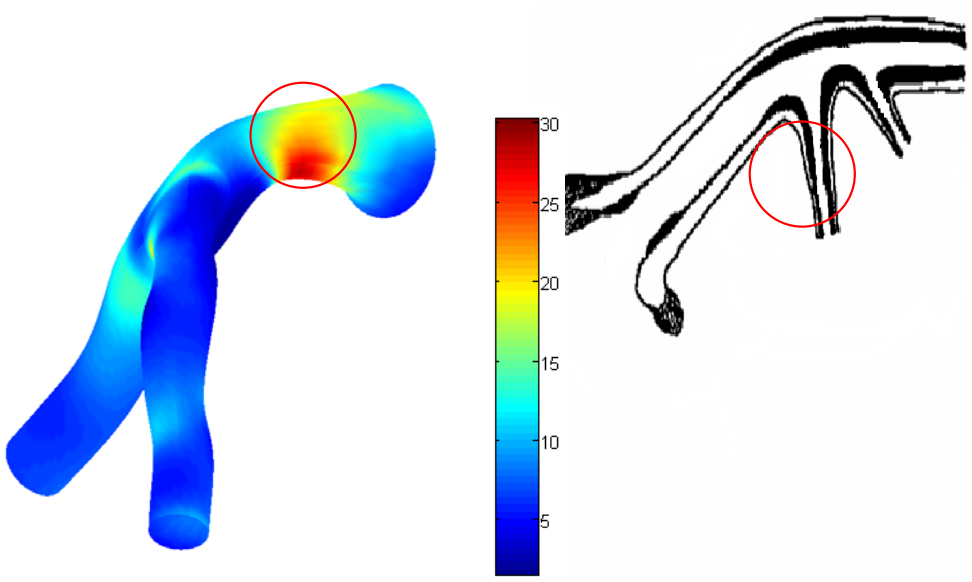

Figure 6: Mean WSS distribution as Figure 4 shows. The region with higher WSS (red circle in the left panel) matches with the region found by Velican, C. and Velican, D. (5) to be "resistant" to atherosclerosis (red circle in the right panel).

This investigation does not consider plaque progression, inasmuch as the CFD model was developed from a normal individual and the clinical data used for comparisons were obtained from autopsy specimens of subjects who died from non-cardiovascular causes. It is intriguing (and as yet unproven) to consider the implications of the low mean/oscillatory WSS hypothesis (LMOSS) to plaque progression. Plaques initially do not encroach upon the lumen, but the ability of the artery to remodel and compensate for plaque growth ultimately cannot counteract lumen reduction. This obviously alters the local geometry, and a stenotic plaque will experience a higher WSS in the narrowed lumen due to increased local velocities – at least until the stenosis becomes flow-reducing. Thus, continued area reduction or plaque rupture may not be directly related to LMOSS. However, flow exiting a stenosis may create a LMOSS region in the distal region of the plaque due to post-stenotic flow separation (25). Perhaps longitudinal plaque progression may be related to this altered environment.

In summary, the results of this investigation are consistent with the hypothesis that early atherosclerotic plaques in the proximal segments of human coronary arteries localize at sites where the hemodynamic WSS is relatively low and oscillates in direction during the cardiac cycle. However, studies are needed that examine both hemodynamics and pathophysiology of individual subjects, noninvasively or minimally invasively, in order to be able to elucidate *in vivo* mechanisms and to translate findings to clinical utility.

Acknowledgement: This research was partially supported by funds from grants NIH NHLBI U01 HL080711 and R01 HL70531. The senior author is a Georgia Research Alliance Eminent Scholars.

References

1. Centers for Disease Control and Prevention (1999) National Center for Health Statistics and National Center for Chronic Disease Prevention and Health Promotion 1999.

2. DeBakey, M.E., Lawrie, G.M., & Glaeser, D.H.(1985) *Ann Surg* **201**, 115-131.

3. Cornhill, F. J., Herderick, E. E., & Stary, C. H. (1990) *Monographs on Atherosclerosis* **15**, 13-19.

4. Fox, B., James, K., Morgan, B., & Seed, A. (1982) *Atherosclerosis* **41**, 337-347.

5. Velican, C. & Velican, D. (1984) *Atherosclerosis* **50**, 173-181.

6. Suo, J., Oshinski, J.N., & Giddens, D. (2003) *J Biomech Eng* **125**, 347-354.

7. Weber, O.M., Martin, A.J., Higgins, C.B., (2003) *Magn Reson Med.* **50**, 1223-1228.

8. Johnson, K., Sharma, P., Oshinski, J. (2007) *J Biomech.* Nov 21 [Epub ahead of print]).

9. Kolodgie, F.D., Burke, A.P., Farb, A., et al. (2001) *Curr Opin Cardiol* **16**, 285-292.

10. Kolodgie, F.D., Virmani, R., Burke, A.P., et al. (2004) *Heart* **90**, 1385-1391.

11. Cheruvu, P.K., Finn, A.V., Gardner, C., et al. (2007) *J Am Coll Cardiol* **50**, 940-949.

12. Wang, J.C., Normand, S.L., Mauri, L., & Kuntz, R.E. (2004) *Circulation* **110**, 278-284.

13. Gibson, C.M., Kirtane, A.J., Murphy, S.A., et al. (2003) *J Thromb Thrombolysis* **15**, 189-96.

14. Malek, A.M., Alper, S.L., & Izumo, S. (1999) *JAMA* **282**, 2035-2042.

15. Suo, J., Ferrara, D.E., Sorescu, D., Guldberg, R.E., Taylor, W.R., Giddens, D.P. (2007) *Arterioscler Thromb Vasc Biol* **27**, 346-351.

16. Cheng, C., Tempel, D., van Haperen, R., et al. (2006) *Circulation* **113**, 2744-2753.

17. Oshinski, J.N., Curtin, J.L., & Loth F. (2006) *J Cardiovasc Magn Reson* **8**, 717-722.

18. Oshinski, J.N., Ku, D.N., Mukundan, S., Jr., Loth, F., & Pettigrew, R.I. (1995) *J Magn Reson Imaging* **5,** 640-7.

19. Gertz, S.D. & Roberts, W.C. (1990) *Am J Cardiol* **66**, 1368-1372.

20. Badimon, L., Badimon, J.J., Galvez, A., Chesebro, J.H., & Fuster V. (1986) *Arteriosclerosis* **6**, 312-320.

21. Jalali, S., Li, Y.S., Sotoudeh, M., et al. (1998) *Arterioscler Thromb Vasc Biol* **18**, 227-234.

22. Groen, H.C., Gijsen, F.J., van der Lugt, A., et al. *Stroke* **38**, 2379-2381.

23. Giddens, D.P., Zarins, C.K., & Glagov, S., (1993) *J Biomech Eng* **115**, 5885-5894.

24. Svindland, A. (1983) *Atherosclerosis* **48**, 139-145.

25. Lieber, B.B. & Giddens, D.P. (1990) *J Biomechanics* **23**, 597-605.